On the Timing and Nature of the Multiple Phases of Slope Instability on Eastern Rockall Bank, Northeast Atlantic

A. Georgiopoulou[1,2], S. Krastel[3], N. Finch[1], K. Zehn[3], S. McCarron[4], V.A.I. Huvenne[5], P.D.W. Haughton[1,2] and P.M. Shannon[1,2]

[1]UCD School of Earth Sciences, University College Dublin, Ireland

[2]UCD Earth Institute, University College Dublin, Ireland

[3]Institute of Geosciences, Christian-Albrechts-Universität zu Kiel, Kiel, Germany

[4]Maynooth University, Department of Geography, Co Kildare, Ireland

[5]National Oceanography Centre, Southampton, University of Southampton Waterfront Campus, SO14 3ZH, United Kingdom

Corresponding author: Aggeliki Georgiopoulou (aggie.georg@ucd.ie)

Key Points:

- Large-scale submarine landslides observed on open slopes are more likely the composite of smaller-scale more frequent slope collapses.
- Slides originating from the same source area can display different types of deposits indicating that the flows had different rheologies.
- To distinguish separate slide events in a slide complex an extensive and diverse high-resolution dataset is necessary.

Abstract

One of the most challenging tasks when studying large submarine landslides is determining whether the landslide was initiated as a single large event, a chain of events closely spaced in time or multiple events separated by long periods of time as all have implications in risk assessments. In this study we combine new multichannel seismic profiles and new sediment cores with bathymetric data to test whether the Rockall Bank Slide Complex is the composite of multiple slope collapse events and, if so, to differentiate them. We conclude that there have been at least three voluminous episodes of slope collapse possibly separated by long periods of slope stability, a fourth, less voluminous event, and a possible fifth more localized event. The oldest event is estimated to be several hundred thousand years old. The second event took place at the same location as slide A, reactivating the same scar, nearly 200 ka ago. Slide C, the most voluminous event, took place 22 ka ago and initiated further north from the other slides. Slide D was of a much smaller event is that happened 10 ka ago while the most recent event, albeit very small-scale, took place within the last 1000 years. This study highlights the need to thoroughly investigate large slide complexes to evaluate the event sequencing as seismic studies may hide multiple small-scale events. It also reveals that the same slide scarps can be reactivated and generate slides with different flow behaviors.

Plain Language Summary

When studying large underwater landslides, determining whether what we see in our data was created by one large event or several smaller events is very difficult due to the inaccessibility of the deep sea. But being able to distinguish the different events and their frequency allows for more accurate risk assessments. 40 years ago, a large landslide was discovered in the northeast Atlantic, on the flank of an underwater plateau. Studies since its discovery have been treating it as one large event. With present-day technology and a higher resolution dataset we have discovered that it is composed of several landslides. The most recent, but very small and localized event, happened in the last 1000 years. The one before is happened 10,000 years ago and it was the size of 680,000 Olympic-size swimming pools. Around 22,000 years ago a landslide 250 times bigger slid down the slope. Two more similar size events happened more than 200,000 years ago, but the further back in time we go the data resolution gets poorer. We think that the sizes of large underwater landslides found in the world's oceans and lakes may have been significantly over-estimated, but their frequency may have actually been under-estimated.

1 Introduction

Passive margins are often punctuated by large submarine landslides involving several 10s to 100s km^3 of sediments and affecting 1000s of km^2 of seafloor. Due to resolution limitations of seabed bathymetric and seismic data and depth below seafloor restrictions of shallow coring systems, it is often challenging to distinguish whether such large landslides took place as a single

large event or as several phases that occurred sequentially over a period of time. Imaged slide scars and slide deposits may be the cumulative effect of several episodes of slope instability in the same location but this can be especially difficult to determine if there are no obvious cross-cutting relationships in the scarps or variable scarp degradation and sediment remoulding in the bathymetric data and/or resolvable time in the seismic data between depositional lobes. However, distinguishing between events and being able to calculate the volumes involved in each episode, together with the interval between discrete failures, are of paramount importance in geohazard risk assessment and in particular in modelling landslide-generated tsunamis. For example, Ward and Day (2001) predicted tsunamogenic waves generated by a potential single catastrophic failure of the west flank of the Cumbre Vieja volcano on La Palma in the Canaries that could transit the Atlantic Basin and arrive at the American coasts with wave heights of up to 8 m. However, Hunt et al. (2011), using sedimentary records, demonstrated that collapses on the northern flank of the adjacent island of Tenerife occurred as separate events. They showed that there is a markedly lower tsunamigenic potential where multistage retrogressive failures occur, even where the time interval between individual failures is very short, in the order of a few days. This study focuses on the Rockall Bank Slide Complex (RBSC), a submarine slide complex which lies on the eastern slope of the Rockall Bank offshore western Ireland, facing NW Europe (Fig. 1). Bottom current activity and contourite deposition have been invoked as partially responsible for the slope collapses (Elliott et al., 2010). Buried basement scarps of the Rockall Bank and contouritic deposition across them have both been suggested to play an important role in slope instability by generating differential compaction and pressure gradients and potentially

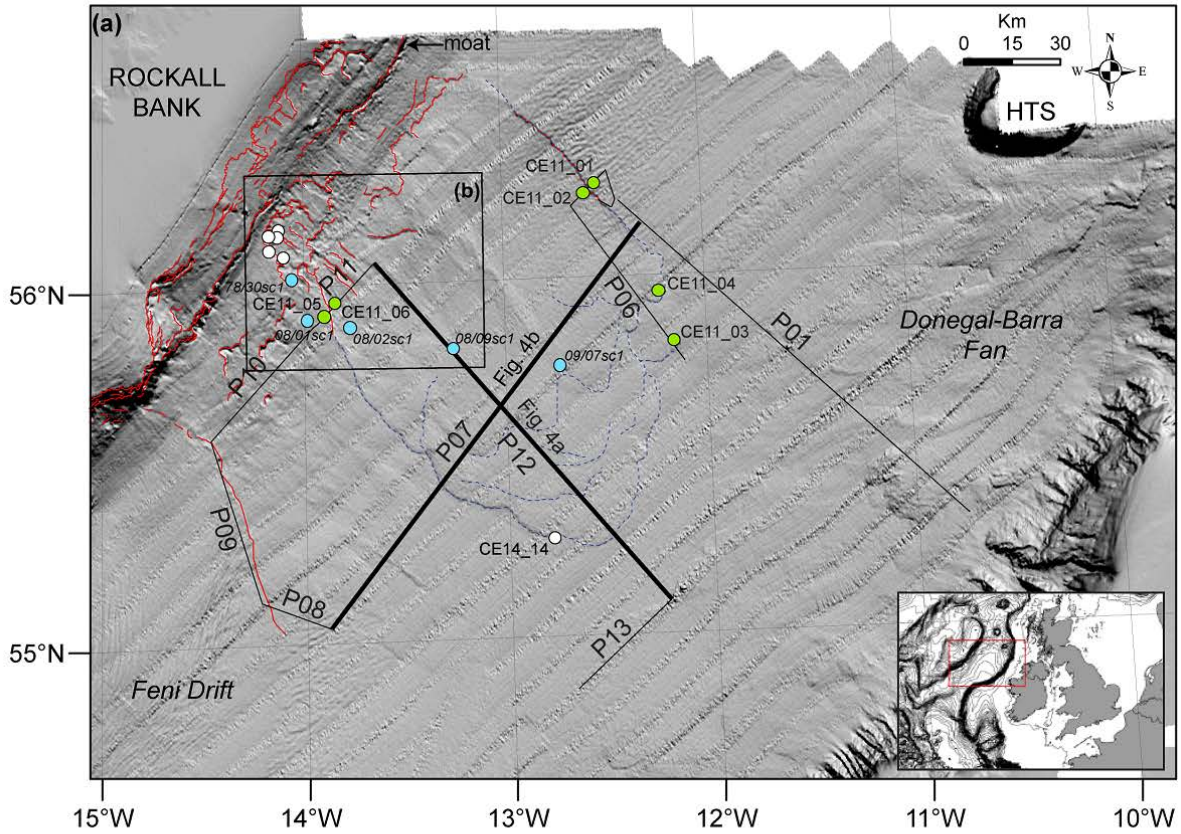
(a)
ROCKALL BANK
moat
Km
0 15 30
N
W
E
S
HTS
(b)
CE11_01
CE11_02
CE11_04
CE11_03
78/30sc1
CE11_05
CE11_06
08/01sc1
08/02sc1
08/09sc1
09/07sc1
Fig. 4b
Fig. 4a
P01
P06
P07
P10
P11
P12
P09
P08
P13
CE14_14
Donegal-Barra Fan
Feni Drift
56°N
55°N
15°W
14°W
13°W
12°W
11°W
10°W

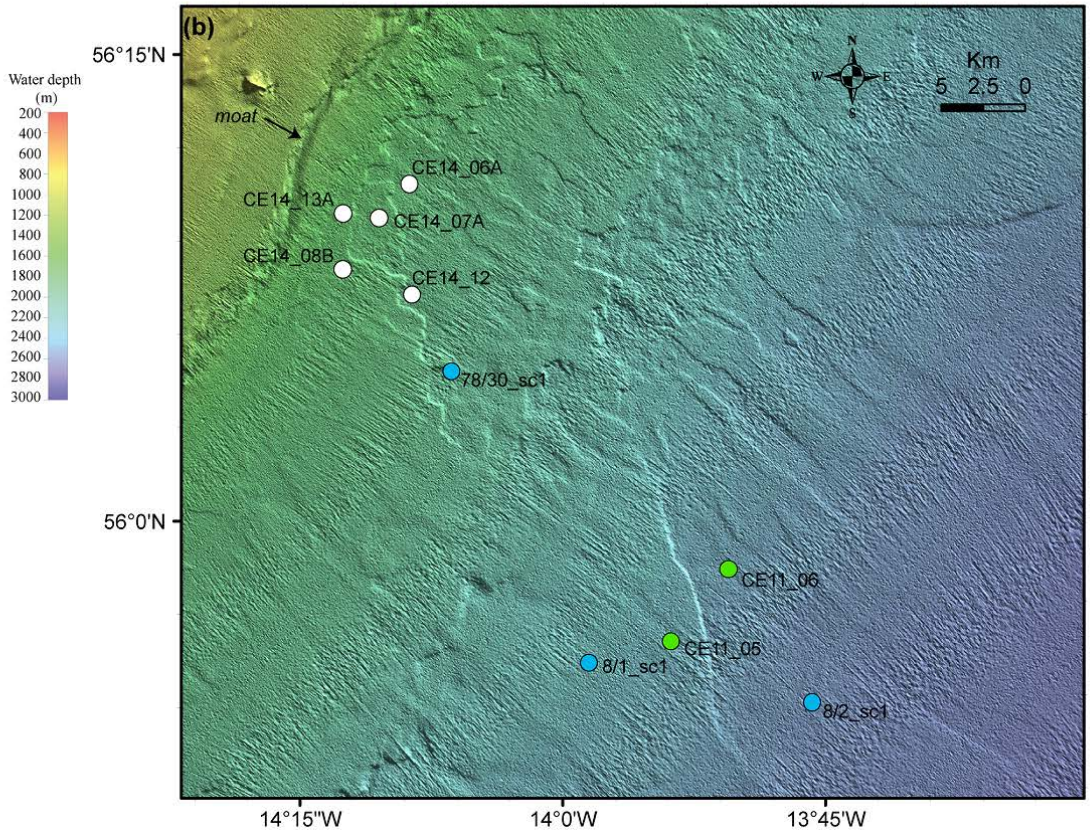
(b)
Water depth (m)
200
400
600
800
1000
1200
1400
1600
1800
2000
2200
2400
2600
2800
3000
56°15'N
56°0'N
moat
N
W
E
S
Km
5 2.5 0
CE14_06A
CE14_13A
CE14_07A
CE14_08B
CE14_12
78/30_sc1
CE11_06
CE11_06
8/1_sc1
8/2_sc1
14°15"W
14°0'W
13°45'W

Figure 1. a) Shaded relief bathymetry map of the northern Rockall Trough offshore western Ireland and data used in this study. The seismic profiles are shown in black and are numbered P01-P13. The locations CE11011 cores are indicated with green circles and of the CE14011 in white circles. The turquoise circles show the locations of the Øvrebø et al. (2005) study. The red lines show scarps associated with the RBSC and the blue dashed lines depict the depositional lobes. HTS = Hebrides Terrace Seamount; b) A zoom in bathymetric map on the location of the lower slope cores. Bathymetric data from the INSS programme.

directing fluid escape towards the seafloor (Georgiopoulou et al., 2013). A study using a traverse of four gravity cores across the RBSC determined with radiocarbon dating that sliding took place during the last glaciation (Øvrebø et al., 2005). Georgiopoulou et al. (2013) suggested that the RBSC probably occurred as a multiphase slope collapse involving at least three episodes, with a potentially incipient or aborted fourth episode. That study relied on indirect evidence from vintage 2D seismic and the INSS (Irish National Seabed Survey) bathymetric data from the scar area. In this paper we use the same bathymetric dataset but we combine it with newly-acquired sediment cores, radiocarbon ages and 2D seismic data from further downslope, in the depositional area of the complex to test Georgiopoulou et al.'s (2013) hypothesis and distinguish the different episodes, evaluate the volumes involved in each, and determine their timing and recurrence interval.

The term "slide" is used in this paper as a generic term for gravity-driven downslope sediment transport and does not infer flow process.

2 Regional Setting

Rockall Trough is an elongate, steep-sided, NNE-SSW trending intracontinental sediment-starved basin west of Ireland and the UK (Fig. 1). It is 200-250 km wide, with water depths from

almost 3000 m in the northern part to more than 4000 m in the south where it opens to the Porcupine Abyssal Plain (Fig. 1).

To the west it is bounded by Rockall Bank, a structural high with an almost flat plateau (0-2^{o}) at <200-400 m water depth and slopes to the east down to 2400 m in less than 90 km with gradients of 5-10^{o}, in places exceeding 15^{o} (Fig. 1).

Deep water masses in Rockall Trough flow northwards along its eastern margin, deflecting anticlockwise at the steepening slopes of the Wyville Thomson Ridge and flow southwards along the base of the Rockall Bank excavating a moat at the base of slope (Fig. 1). Bottom currents are responsible for the redistribution and deposition of sediments to form sediment drifts (Stoker, 1998; Stoker et al., 1998).

Sedimentation rates were as high as 17.1 cm ka^{-1} during the Holocene on the crest of the Feni Drift but were lower (14.6 cm ka^{-1}) during the last glacial period, and significantly less prior to that, averaging 5 cm ka^{-1} for the Pleistocene (van Weering and de Rijk, 1991).

The RBSC truncates a field of sediment waves associated with the Feni Drift. It excavated part of Rockall Bank and deposited sediment onto the floor of the trough (Elliott et al., 2010; Flood et al., 1979; Georgiopoulou et al., 2013; Unnithan et al., 2001) (Fig. 1). Associated scarps have gradients of 30-35° and locally up to 70° (Georgiopoulou et al., 2013). Volumes excavated from the entire scar have been estimated to be between 260 and 760 km^{3} (Georgiopoulou et al., 2013). The glide plane for the RBSC is believed to be the regional intra-early Pliocene C10 unconformity (Elliott et al., 2010). The sedimentary sequence between C10 and the present-day seafloor outside of the main area of failure (RTa in Stoker et al., 2001) comprises alternating debris flow deposits and parallel- to wavy-bedded drift accumulations, locally disrupted by slope failure deposits (Stoker et al., 2001).

3 Data and Methodology

Our study is based on 13 new multi-channel high-resolution seismic profiles (a total of c. 700 line km), six new piston cores collected during RV Celtic Explorer cruise CE11011, five new gravity cores collected during the SORBEH CE14011 expedition (Slope Collapses on Rockall Bank and Escarpment Habitats), four gravity cores from Øvrebø et al. (2005), integrated with open-access bathymetric data that had been acquired as part of the INSS programme (Irish National Seabed Survey) between 2000 and 2001 on R.V. Bligh (Fig. 1). The multibeam bathymetry was collected using a Simrad EM120 multibeam echo-sounder with frequencies of 11.75–12.75 kHz. A detailed account on the processing of the multibeam data can be found in Sacchetti et al. (2012a).

The seismic source used for acquiring the seismic data was a Mini-GI Gun. The gun was shot in true GI-Gun mode with a volume of 0.2l for the generator and 0.4l for the injector. The main frequency is ~200 Hz. The injector was triggered with a delay of 20 ms after the generator to suppress the bubble signal in the recorded seismic data. The shooting rate was 9 seconds resulting in a shot point distance of ~20m at 4.5 knots boat speed. The gun operation employed a high air pressure of 150 bar (2150 PSI). The data were received by a 187.5 m-long 120-channel long streamer (Geometrics GeoEel); channel spacing was 1.56 m Positioning was based on GPS (Global Positioning System).

The processing procedure included trace editing, setting up geometry, static corrections, normal moveout corrections, filtering , stacking, and time migration. A common midpoint spacing of 5 m was applied throughout. A constant velocity of 1500 m/s was chosen for the NMO-correction

and migration as the streamer was too short for a velocity analysis. Poor weather conditions during acquisition caused a relatively high noise level in the data.

New cores from two different cruises are combined in this study. The CE11011 (CE11) cores were collected using a Geo-piston corer with 110 mm-diameter and 6 m-length barrels. Six cores were collected (Fig. 1) with average retrievals of 3.5 m, with the longest retrieval being 4.29 m below the seafloor. The CE14011 (CE14) cores were collected using a 65mm diameter gravity corer with 3m and 6m-long barrels and average retrieval of 1 and 1.9 m respectively.

The cores were first logged visually for sediment structures, grain size, and colour. They were then logged for physical properties (gamma ray, p-wave velocity, magnetic susceptibility and lightness) in a GeoTek Multi-Sensor Core Logger in split mode setup in the Irish Sediment Core Research Facility at Maynooth University. Selected sandy samples were examined under a binocular microscope for bulk mineralogy comparisons of different sandy intervals. Samples were selected for radiocarbon AMS dating (^{14}C) which was performed on pristine planktonic foraminifera shells of mixed species as there was very little material for monospecific picking. The dating was performed by the Poznań Radiocarbon Laboratory. The results were calibrated using Calib v7.0.4 using the Marine 13 calibration curve (Reimer et al., 2013; Stuiver and Reimer, 1986). A marine reservoir correction was applied based on data from the nearest location of $\delta R=53\pm50$ (Castle Rock, North Channel – Harkness, (1983)).

A total of 23 samples were taken for radiocarbon AMS dating and are supplemented by three more from Øvrebø et al. (2005) (Table 1). The results were calibrated using Calib v7.0.4, based on the Marine 13 calibration dataset (Reimer et al., 2013) (Table 1). Sedimentation rates are calculated between two samples taken from the same core or, where only one sample was taken from the core, between the top of the core taken to be Present Day, i.e. zero yrs BP and the depth

of the sample. This was possible as there is no evidence of erosional features, no significant event beds or major facies changes between the sample depths and we are confident that the seafloor was recovered, usually obvious by the characteristic orange hue of oxidation.

Table 1. Raw radiocarbon data, calibrated ages and resulting sedimentation rates.

Core	depth downcore (cm)	Age 14C (BP)	Calibrated (BP)*		sedimentation rates cm ka^{-1}
CE11_02	210	15,200 ± 80	17,670 - 18,197	**17,940** ± 260	11.7
CE11_03	10	2165 ± 30	1545 - 1838	**1690** ± 150	
CE11_03	22	7360 ± 40	7643 - 7915	**7780** ± 140	
CE11_03	42	13,010 ± 70	14,310 - 15,161	**14,740** ± 430	2.45
CE11_05	73	24,960 ± 190	28,049 - 28,941	**28,500** ± 450	2.56
CE11_06	134	13,830 ± 70	15,806 - 16,333	**16,070** ± 260	
CE11_06	203	18,420 ± 100	21,420 - 22,087	**21,750** ± 330	12.3
CE14_07A	65	10,160 ± 50 BP	8941-9268	**9120** ± 178	7.12
CE14_07A	129	19,590 ± 170 BP	20,630-21,555	**21,092** ± 462	
CE14_07A	156	25,020 ± 190 BP	26,160-27,096	**26,614** ± 454	
CE14_08B	20	19,150 ± 110 BP	20,389-20,933	**20,661** ± 272	
CE14_08B	40	>46,000			
CE14_08B	64	>46,000			
CE14_08B	64	>46,000			
CE14_08B	187	>46,000			
CE14_08B	192	>46,000			
CE14_08B	237	>46,000			
CE14_12	69	20,400 ± 120	21,697-22,378	**22,037** ±340	3.13
CE14_12	121	>46,000			
CE14_12	162	>46,000			
CE14_13A	29	9820 ± 50	8550-8969	**8760** ± 209	3.3
CE14_13A	64	20,590 ± 120	21,928-22,569	**22,248** ± 320	
8/9_sc1	90	9500 ± 55	10,099 - 10,305	**10,202** ± 103	
8/9_sc1	120	>46,000			
9/7_sc1	160	20,540 ± 140	23,317 - 24,189	**23,753** ± 436	
9/7_sc1	200	18,800 ± 120	21,383 - 22,106	**21,744** ± 361	

* delR = 53 ± 50

The last column is expressing the average value from column D but with ± instead of min - max.

Made by [(max-min)/2 + min ± (max-min)/2] and rounded to the nearest 10th

Calibration Stuiver et al 1998

4 Results and interpretation

4.1 Bathymetry

The planform morphology of the RBSC has been described in several previous studies (Elliott et al., 2010; Flood et al., 1979; Georgiopoulou et al., 2013; Sacchetti et al., 2012a,b), so only a brief summary is provided here with an emphasis on the lower slope and insights from the newly-acquired seismic data. On the basis of different degrees and styles of deformation, the upper slope where the scars of the RBSC are found, was divided into the Upper slope region and the Lower slope region which are separated by an alongslope moat that strikes parallel to the base of slope (Georgiopoulou et al., 2013). The Upper slope region was further subdivided into the North, Central and South regions, which demonstrate very different scarp characteristics; the North has rough-edged, arcuate scarps up to 150 m high, whereas the South is dominated by cuspate, bite-shaped, smooth-edged scarps also up to 150 m high (Georgiopoulou et al., 2013). Strikingly different is the Central area, where there are at least three scars, much shallower, up to 20 m high, separated by flat-topped ridges (Georgiopoulou et al., 2013). The total width of the upper slope area that is affected by scarps is 120 km (Fig. 1).

Downslope of the moat, <5km, the Lower slope region is severely scarred by multiple intersecting scarps (Fig. 1) (Georgiopoulou et al., 2013). Here, the RBSC is clearly still erosional and its margins are defined by truncations of the sediment wave fields of the Feni Drift, along the south and the north sidescarps (Fig. 1). Cores CE11_01 and _02 have targeted the northern sidescarp, with CE11_01 serving as a reference core from the undisturbed seafloor and CE11_02 taken inboard of the scarp (Fig. 1a). There are a number of other sidescarps within this area, downslope of the Lower slope region. Planar terraces at different stratigraphic levels can be identified here and a flow fabric is observed downslope from them with elongate linear furrows,

ridges defining a conical-shaped erosional region opening downslope (Fig. 1b). The CE14 cores targeted these terraces (Fig. 1b).

In the distal/depositional area the seafloor is occupied by a set of overlapping lobes, which at the toe of the complex have sharp, up to 25 m high, frontal margins. Cores CE11_03, CE11_04 and CE14_14 have targeted the terminations of these lobes (Fig. 1).

4.2 Seismic facies and their distribution

The newly-acquired multichannel seismic profiles provide a higher resolution of the sub-seafloor sequence than previously seen on the legacy industry seismic profiles (e.g. (Elliott et al., 2010; Georgiopoulou et al., 2013). The new data reveal that the acoustic character of the sediments is highly variable both laterally and vertically. Five seismic facies have been identified and mapped (Figs 2 and 3).

- Facies 1 comprises parallel, wavy, continuous reflectors of moderate to strong amplitude. The wavelength is between 1 and 2.6 km and the amplitude 5-10 m. This facies, consisting of interbedded lithologies giving it its characteristic “striped” appearance, is interpreted as the deposits of sediment waves created by bottom currents. Their distribution coincides with sediment waves interpreted previously from bathymetric and seismic data (Elliott et al., 2010; Sacchetti et al., 2011; Sacchetti et al., 2012b), while the scale range generally agrees with the size of bottom current-related sediment waves (Wynn and Stow, 2002). The sediment waves are part of the Feni contourite drift and are

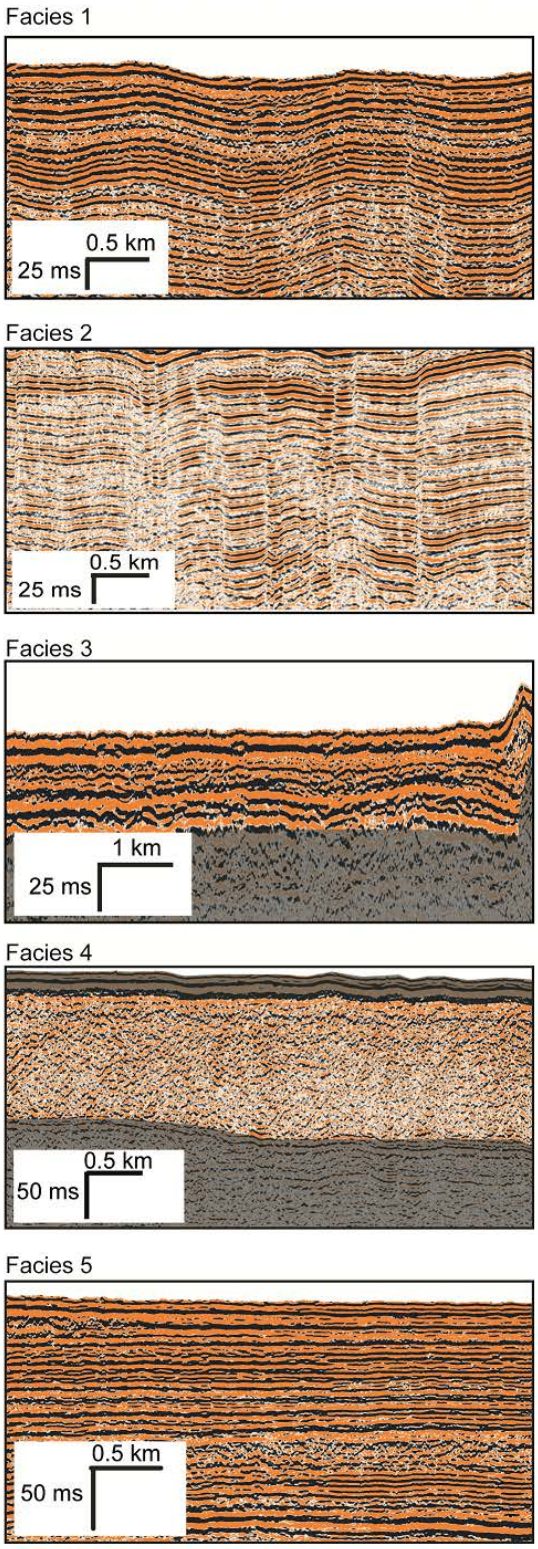

Figure 2. Seismic facies identified on the 13 seismic profiles.

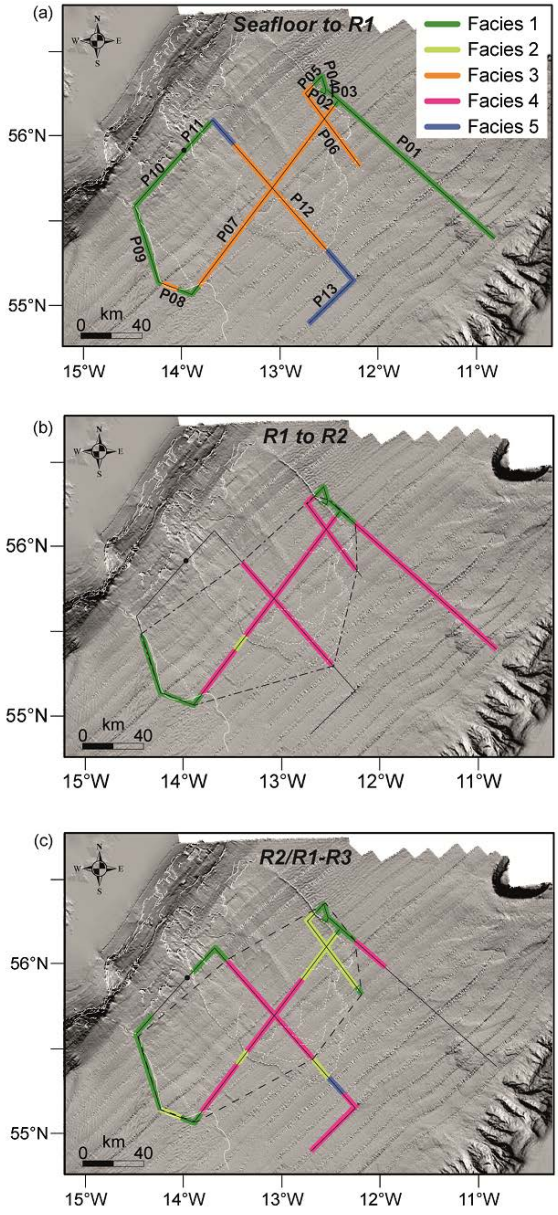

Figure 3. Distribution of the seismic facies on the profiles at different stratigraphic levels. The thin white lines show the scarps and depositional lobes of the RBSC. (a) Between the seafloor and Reflector 1, (b) between Reflector 1 and Reflector 2 and (c) between R2 (and where it missing R1) and reflector R3. The dashed and dotted line in

(b) and the dashed line in (c) show the mapped extent of R2 and R3 respectively (see also fig. 5).

sharply truncated by the RBSC scarps (Faugères et al., 1999; Flood et al., 1979; Sacchetti et al., 2011).

- Facies 2 is characterized acoustically by weak to moderate amplitudes, and contains parallel semi-continuous reflectors. This facies is also interpreted as generated by sediment waves but within the scarps in the northern RBSC-affected area in the deeper sedimentary sequence (Fig. 3c) which explains the weakening of the seismic amplitude. They are sharply truncated to the southwest by a scarp. This relationship has implications on the timing of the RBSC events and will be discussed further in section 4.5.
- Facies 3 shows sub-parallel, partly discontinuous, irregular reflectors with high amplitudes. Facies 3 sediments are interpreted as draping hemipelagic sediments, possibly punctuated by turbidites, healing the topography left by the RBSC, as in most cases it is found covering facies 4.
- Facies 4 is acoustically chaotic to transparent with little discernible structures or reflectors. Facies 4, which occupies mostly areas within the RBSC limits (scarps and lobes) near the surface and at depth, represents deformed slope sediments. The acoustic character demonstrated in this facies (transparent, chaotic reflectors) is typical of slide deposits (e.g. Bull et al., 2009; Sacchetti et al., 2012a). The extent of this seismic facies suggests that slide deposits are present beyond the confines of the RBSC limits as seen on the seafloor, to the east (Fig. 4). This is coincident with the southwestern reaches of the glacially-fed Donegal-Barra Fan that is sourced from the northeast Rockall Trough margin and is almost entirely composed of debrites and mass transport deposits (Georgiopoulou et al., 2012; Holmes et al., 1998; O'Reilly et al., 2007; Sacchetti et al., 2011).

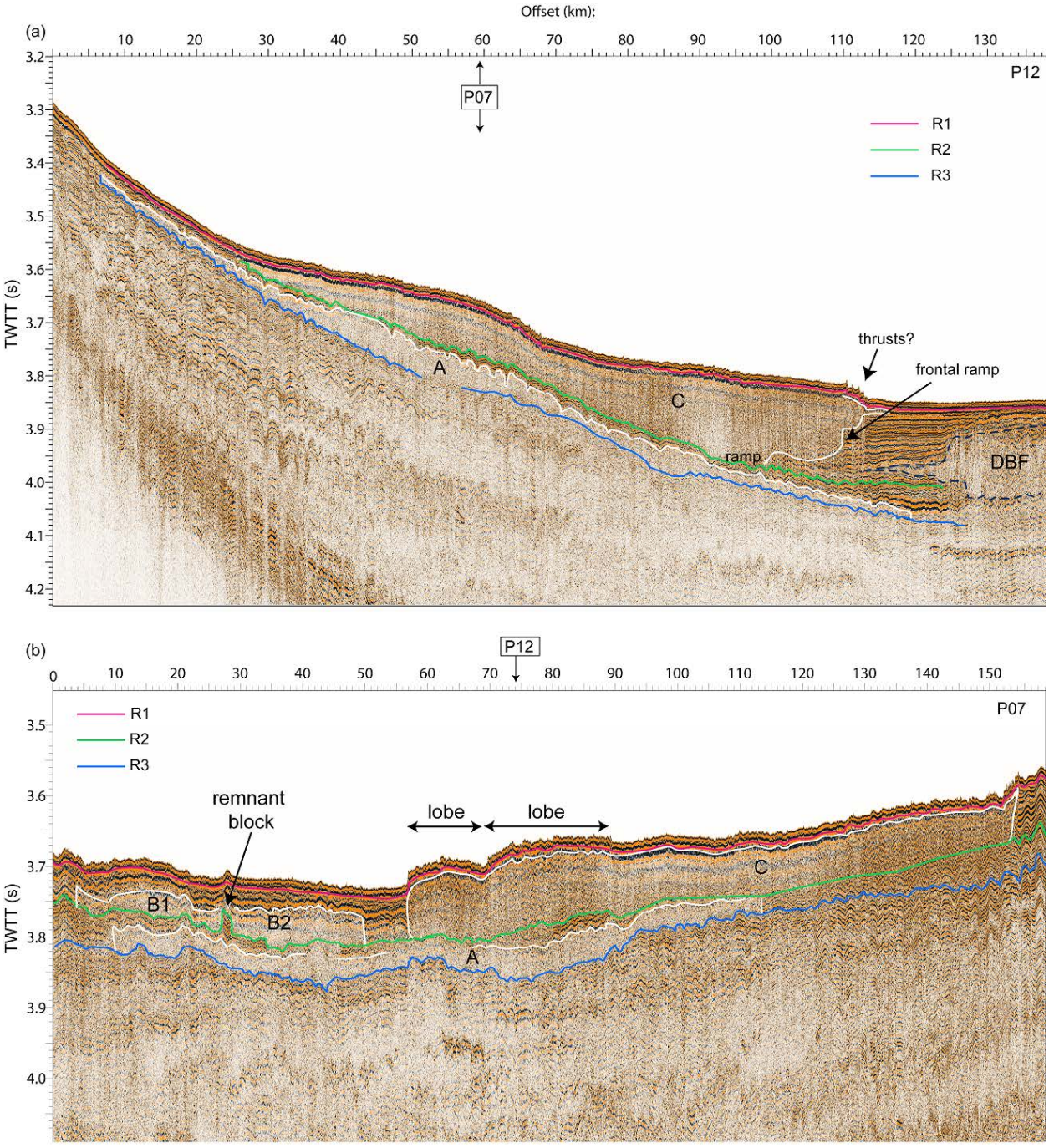

Figure 4. Seismic profiles (a) P07 along the length of the RBSC lobes and (b) across the RBSC lobes (for location see fig. 1). Reflectors R1-R3 are shown in magenta, green and blue. White lines are showing the upper and lateral limits of slide bodies. The profiles cross where indicated in each figure with an arrow.

- Facies 5 shows parallel, mostly continuous reflectors of high amplitude. Facies 5 is similar to facies 1 in being characterized by a continuous layered seismic character. However, it cannot represent sediment waves as it lacks the undulating character of facies 1. On the other hand, given the similarity of the acoustic character, the lithologies are likely to be similar to those of facies 1 and similarly with facies 3 are interpreted as hemipelagic sediments with interbedded turbidites. Sediment cores from the near-surface that have been collected in the area of facies 5 distribution confirm the presence of intercalated hemipelagic sediments with sandy turbidite beds (Georgiopoulou et al., 2010; Georgiopoulou et al., 2012).

Three seismic horizons have been mapped on most seismic profiles (Fig. 4), based on their spatial continuity and their positioning relative to the acoustic facies distribution. Horizon 1 (R1) defines the surface post-failure sediments and is mapped at about 20-30 ms below the seafloor throughout the survey. R1 is mostly continuous, only in places patchy, with low-to-moderate amplitude. R1 is widespread and could be mapped on all profiles (Fig. 5a). The surface sediments that lie between R1 and the seafloor are mostly high amplitude continuous reflectors of facies 1 and 5 outside the RBSC sidescarps and mostly facies 3 within the scarps (Fig. 3a). An area of facies 1 stretches within the scar near the base of slope along profiles P10 and P11 (Fig. 3a).

Horizon 2 (R2) is a moderate-amplitude, continuous reflector that is found in the central and northern part of the survey (Fig. 5b). It is less widespread than R1, with clear terminations within the study area; it shallows upslope and downslope towards R1 and is sharply truncated on profile P01 (Fig. 5b). Between R1 and R2 the most prevalent facies is facies 4, at least within the RBSC affected area, where it pinches out both upslope and downslope (Fig. 3b). Outside the sidescarps

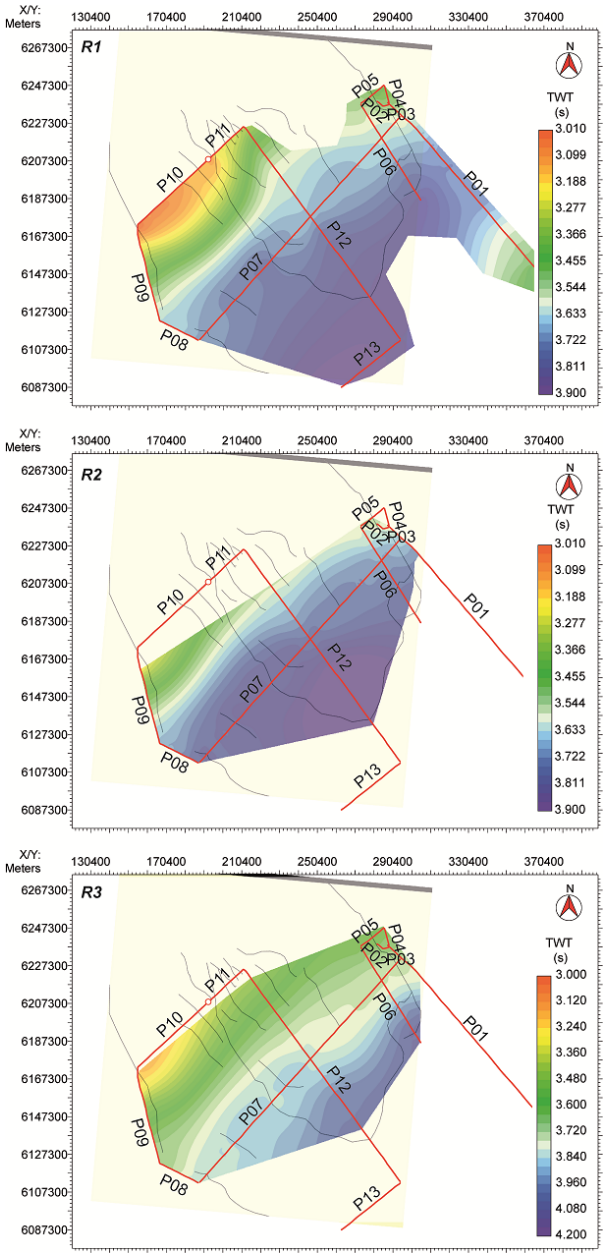

Figure 5. Maps of the three reflectors maps. Note the widespread distribution of R1 in (a) and the limited distribution of R2 (b) relative to both R1 (a) and R3 (c).

facies 1 is continuous from the seafloor down to the level of R2 and below (Fig. 4b). Facies 4 is also found beyond the RBSC-affected area as seen on profile P1 which traverses the depositional lobes of the Donegal Barra Fan (Figs 3b and c).

Horizon 3 (R3) is an irregular moderate amplitude reflector that is fairly continuous and mapped throughout most of the survey (Figs 4 and 5c). On profile P12 the quality of the seismic deteriorates southeastwards and it is impossible to map the reflector and in P01 it is abruptly truncated against facies 4. Facies 4 and 2 are found between R3 and R2: facies 4 mostly in the central and southern area and facies 2 in the northern edge, against the northern sidescarp (Fig. 3c). Outside the limits of the RBSC facies 1 continues to be dominant in the R2-R3 interval (Fig. 3c).

4.3 Sedimentary facies

Four main sedimentary facies are identified (Fig. 6) in the cores as follows:

- HM are muds, further divided into two sub-facies; HM1, a light coloured silty, foraminifera-bearing mud and HM2, a dark coloured, mottled, foraminifera-poor, clayey mud. Their physical properties do not differ much; they show only very subtle differences in p-wave velocity and gamma-ray density, while magnetic susceptibility seems to be higher in HM2. Both subdivisions of Facies HM are found in all cores (Fig. 7).
- CD are clast-supported debrites and can be found in cores CE11_05 and 06, CE14_12, _13A and 06A, and cores 8/9sc1 and 78/30sc1 (Fig. 7a).
- Facies SD represents deformed layers that may be sheared, folded or disrupted. For example, there is a section of CE11_03, between about 80 cm to 175 cm downcore, which appears deformed (Fig. 7b). The deformation cannot be attributed to coring

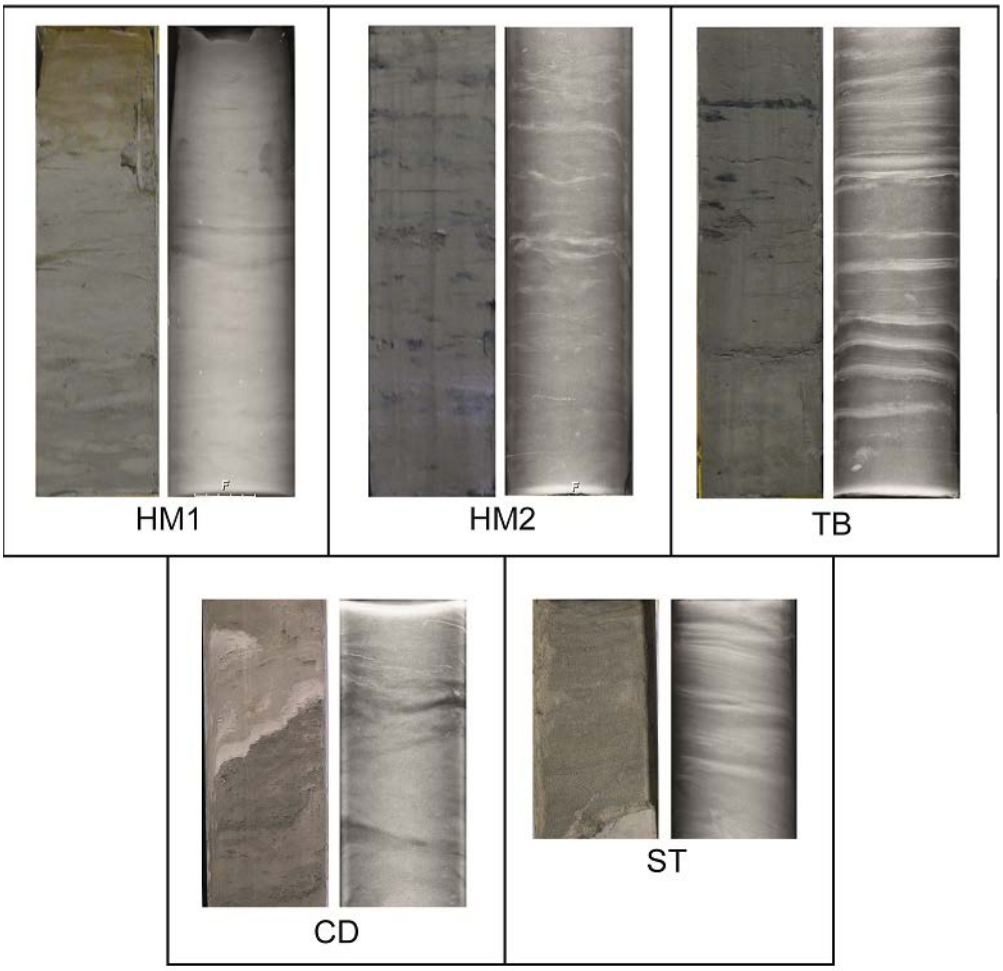

Figure 6. Sedimentary facies identified in the cores. Figure on the left and x-ray on the right for each of the sedimentary facies. See text for more details.

problems as it is not pervasive. However, even though it is deformed it does not appear to be mixed.

- ST are sandy layers (fine to medium sand size), often fining upwards. In several of the cores this facies sits directly on top of CD. In most cases, the sandy layers appear laminated, better visible in the x-rays (Fig.6). Where lamination is not present the layers appear disturbed and fluidized, which may suggest destruction of the original structures. They are characterized by increases in p-wave velocity, gamma-ray density and magnetic susceptibility (Fig. 7).
- TB are thinly bedded silt-fine sand layers in dark clayey mud background (Fig. 6). Facies TB is only seen in cores near the axis of the trough CE11_03, CE11_04 and CE14_14, but is significantly thicker in CE11_03 (Fig. 7a). In this interval the physical properties, particularly the gamma-ray density and magnetic susceptibility, appear erratic, but the pattern seems to suggest increases for both parameters in the coarser layers (Fig. 7a).

Facies HM is interpreted as background hemipelagic sediments with different degrees of bioturbation, mostly by Zoophycos. The two subdivisions, HM1 and HM2, are similar to the GM and BM facies reported in deeper water by (Georgiopoulou et al., 2012). Like that study, and based on radiocarbon dating (Fig. 7), we interpret HM1 to represent sediments deposited during the current interglacial, which explains the higher foraminifera content and the light colour, indicative of higher carbonate content and therefore higher productivity. The darker muds with the black staining and paucity of foraminifera were deposited during the last glacial, confirmed also by the dating (Fig.7). The age of the transition from the last glacial to the current interglacial according to the radiocarbon data is 13 ka (based on CE11_03). The high degree of bioturbation

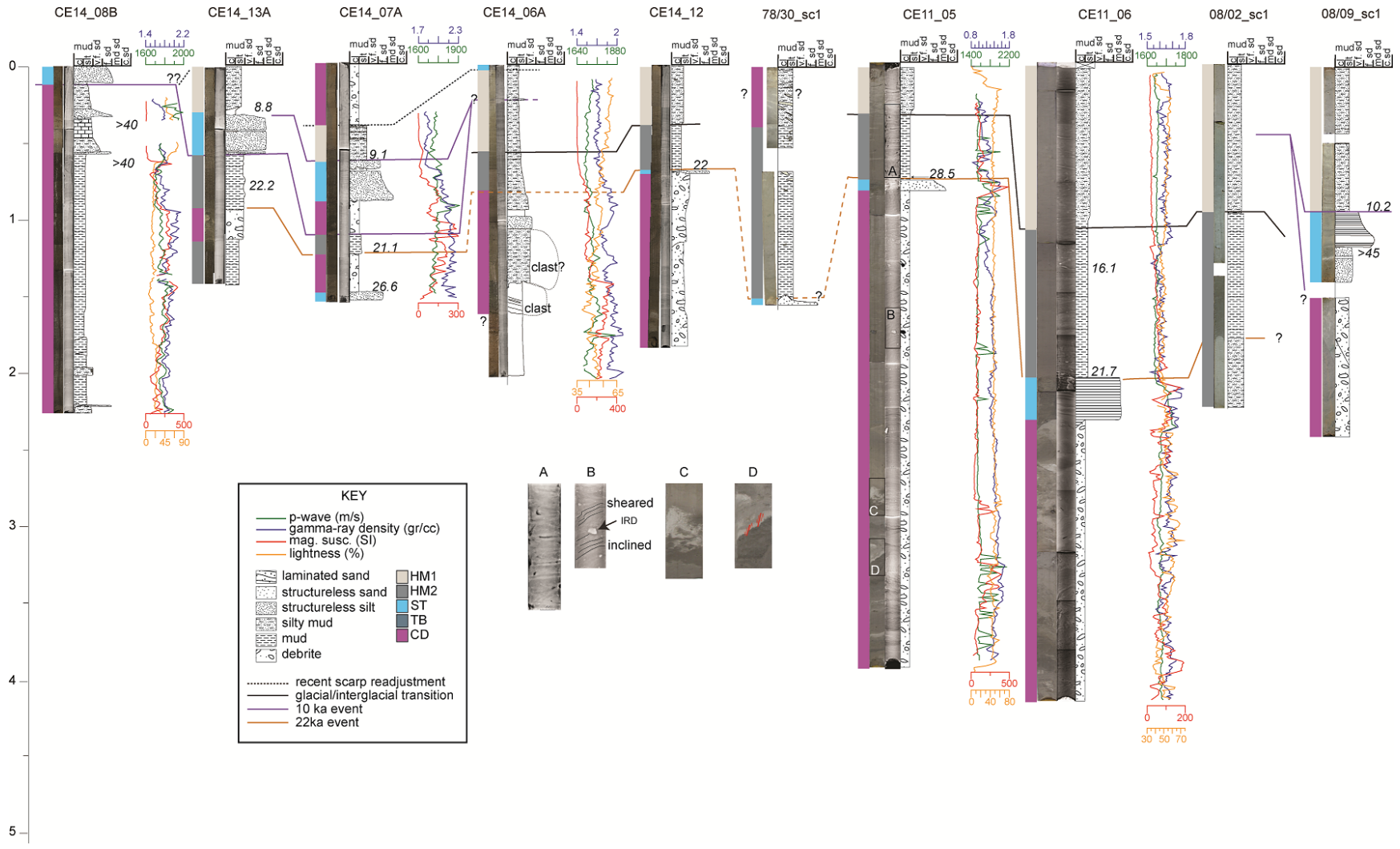
CE14_08B
CE14_13A
CE14_07A
CE14_06A
CE14_12
78/30_sc1
CE11_05
CE11_06
08/02_sc1
08/09_sc1
>40
>40
8.8
22.2
9.1
21.1
26.6
clast?
clast
22
28.5
16.1
21.7
10.2
>45
A
B
C
D
sheared
IRD
inclined
KEY
p-wave (m/s)
gamma-ray density (gr/cc)
mag. susc. (SI)
lightness (%)
laminated sand
structureless sand
structureless silt
silty mud
mud
debrite
HM1
HM2
ST
TB
CD
recent scarp readjustment
glacial/interglacial transition
10 ka event
22ka event

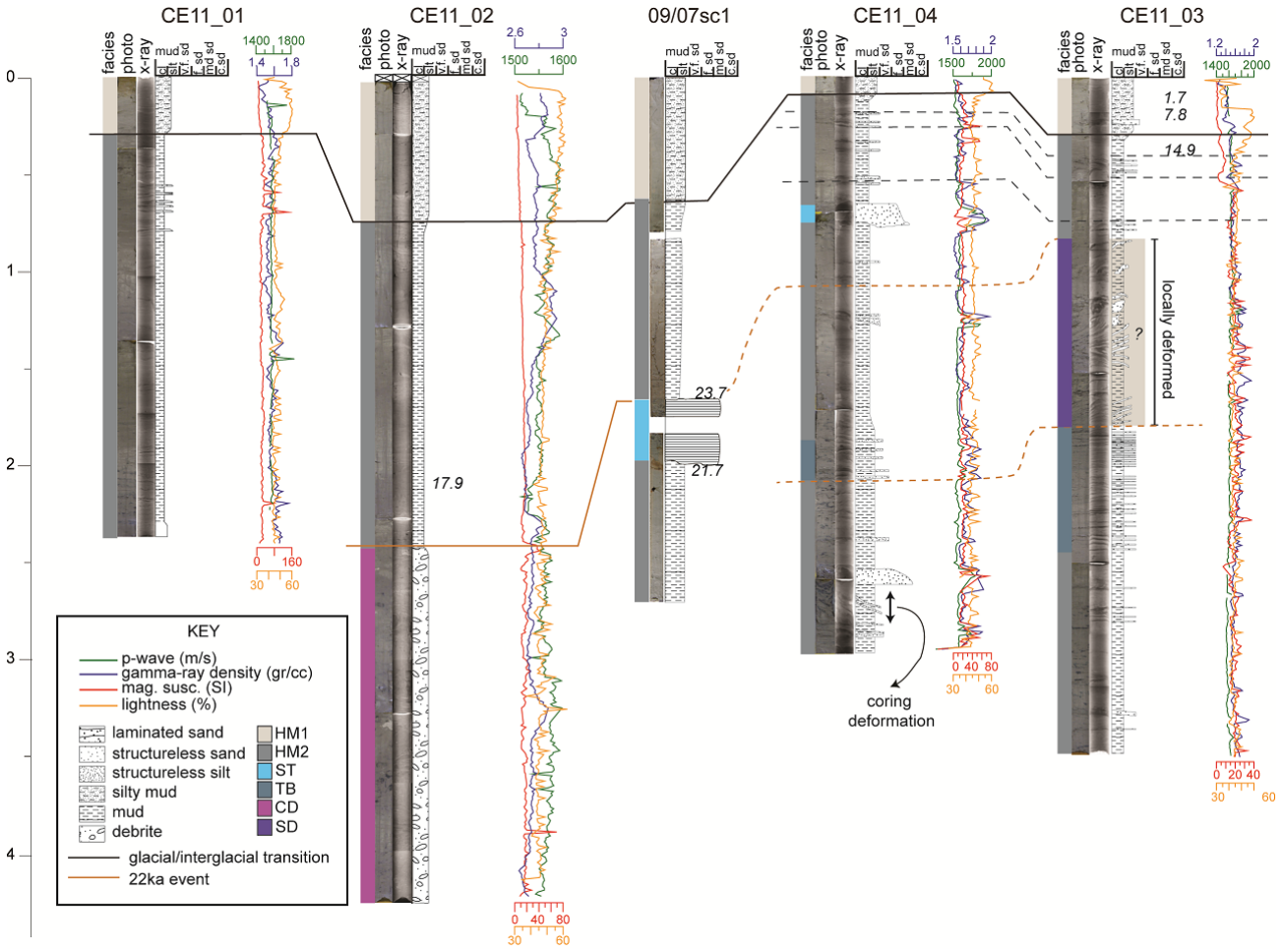

Figure 7. a) Correlation panel of the lower slope cores, parallel to the flow axis; b) correlation panel of the cores along the northern edge of the RBSC. For each core we show the photo, x-ray (where available), lithological log, facies interpretation and physical properties (where available). Solid lines show confident correlations whereas dashed lines are inferred correlations and extensively discussed in the text. The ages (italics) are shown in years Before Present (BP). Insets A-D are blow-ups of the photo and x-ray from core CE11_05, and show in more detail the internal deformation in the debrite. Note the very small increase in density at 240cm

downcore in CE11_05; if two separate debrites were stacked the density at their contact would be expected to show a significant increase to the right. The coring disturbance indicated in core CE11_04 took place during extraction of the core from the barrel.

through HM1 is attributed to interglacial burrowing activity as evidenced by the light grey HM1 mud that has been mixed with the darker HM2 mud.

Facies TB, that can be found only in CE11_03, _04 and CE14_14, which are the cores closest to the axis of the Rockall Trough and nearest the Irish margin, is interpreted as fine grained-turbidites originating from meltwater plumes from the British Irish Ice Sheet (BIIS) that was covering the Irish shelf to the east of the study area at the time (Peters et al., 2016). They correspond to the turbidites that are found as thicker and slightly coarser sequences in cores more proximal to the Irish slope (Georgiopoulou et al., 2012), but they are not found in cores closer to Rockall Bank. Rockall Bank was likely too distal for these turbidity currents and is also in shallower waters.

The clast-supported character of facies CD indicates this is a debrite composed of clasts of multiple lithologies. This is the same character as reported by Faugères et al. (1981) and Øvrebø et al. (2005).

The section 83-240 cm in CE11_05 that corresponds to facies SD is remarkably different when compared with the interval immediately below it in that it is not composed of multiple clasts. Instead it appears similar to the glacial background sediments, but the bioturbation is deformed, there are some small (1-2cm dimeter) clasts floating in the mud, and the x-rays show sheared and inclined layers (Fig. 7a). These two sections can either be described as two debrites that are stacked or infer that the interval 83-240 cm is a larger clast within the debrite. We prefer the second interpretation as there is no sharp change in the gamma-ray density log (Fig. 7a), where the second debrite would be shearing and depositing on top of the older one, causing compression and/or eroding into deeper-buried strata with increased in density.

The debrite is capped by facies ST in CE11_05 and _06 (Fig. 7a). We interpret this to be a co-genetic turbidite that deposited from a more dilute suspended flow through debris flow transformation or mobilized at the same time as the debris flow. This relationship was also observed in the nearby gravity core 08/09sc1 of Øvrebø et al. (2005). However the ages of the deposits do not match (Fig. 8) and therefore cannot be correlated. They also correlate with the debrite near the bottom of CE14_07A and the one in CE14_12 (Figs 7a and 8). About 30 km laterally towards the east, neither the debrite nor the turbidite can be correlated into CE11_03 and _04, but stratigraphically they coincide with the top of the disturbed sequence in CE11_03 (Figs 7b and 8). This suggests that either the flow ceased close to the location of 09/07sc1 or that it carried on beyond that location but just did not expand laterally towards the east. Debrite/turbidite events occupying cores CE14_08B and 78/30_sc1 are difficult to correlate with any of the other events and may represent a separate single event.

The timing of emplacement of these debrites and turbidites is discussed further in section 4.5.

4.4 Sedimentation rates

CE11_03 and CE11_05 show relatively slow sedimentation rates (ca 2.5 cm ka^{-1}) compared to CE11_06 and CE11_02 (both about 12 cm ka^{-1}) (Table 1). We believe these differences can be attributed to the location of the cores relative to the route of the bottom current, suggesting that our cores straddle the boundary of the deep water mass that sweeps the base of slope of Rockall Bank. Where the current effect exists, the sedimentation rates are larger, i.e. where cores CE11_02 and CE11_06 were taken from, as opposed to the area where CE11_03 was taken from, beyond the effect of the bottom current. This interpretation is further corroborated by the presence of sediment waves around CE11_02 and CE11_06, but not around CE11_03 (Fig. 1). A problem that arises with this interpretation is that CE11_05 was taken only 5.5 km away from

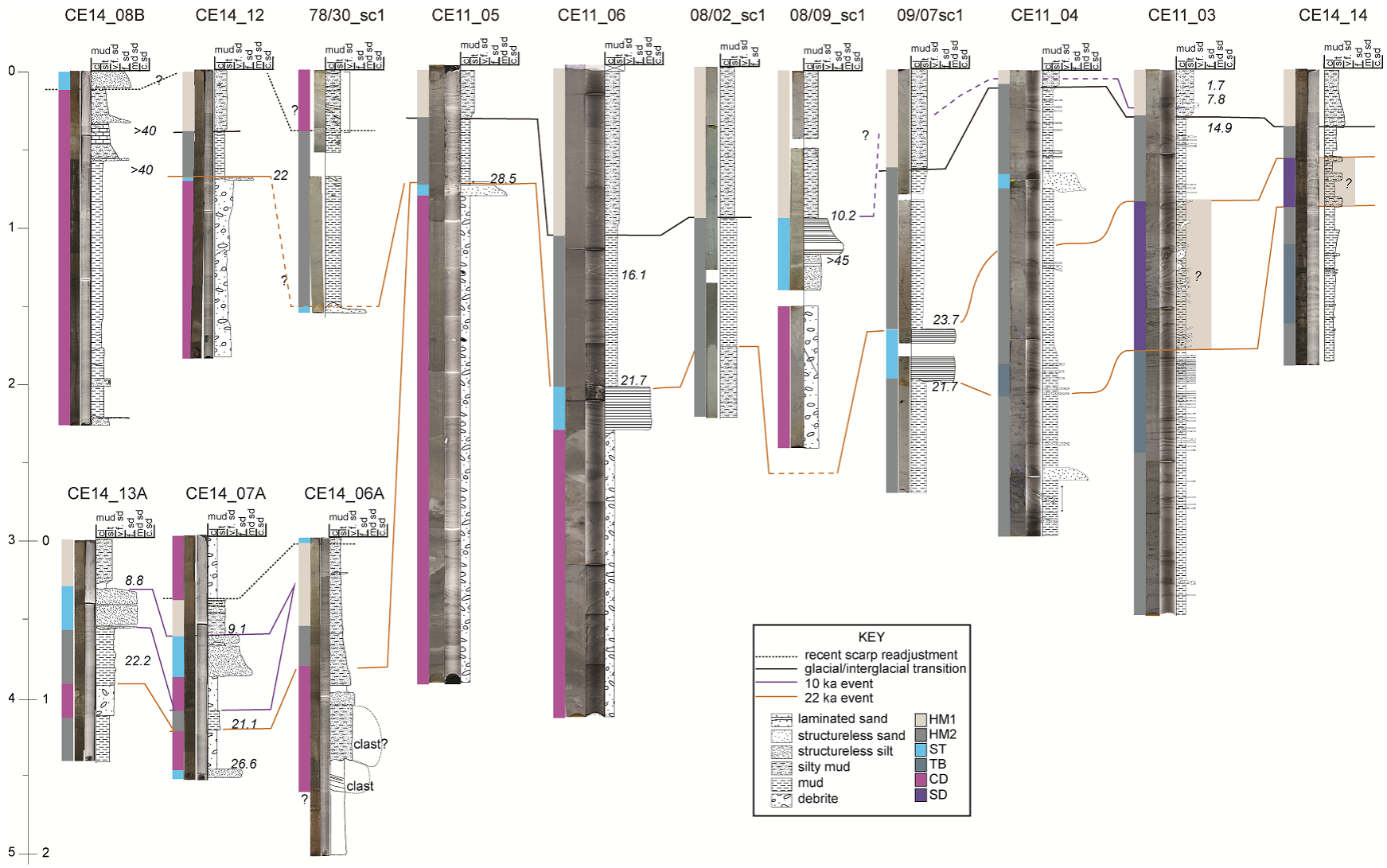

Figure 8. Correlation panel of all the cores used in this study as compiled from figures 7a and b.

CE11_06 and yet the sedimentation rate is nearly an order of magnitude lower. Three reasons can be invoked to explain this difference; (1) the dated sample from CE11_05 contained older material either resulting from the heavy bioturbation evident on the x-ray images or because the top of the sandy layer that forms the cap to the debrite was not completely avoided when sampling; (2) the top one meter of the core is significantly compressed. However, the shape of the trace fossils does not suggest any significant compression, so this possible interpretation is ruled out; (3) sediment was preferentially depositing where there was more accommodation space, and CE11_06 was taken from inside a scar, whereas CE11_05 just outside it. The elevation difference between the two cores is 65 m.

4.5 Evidence of separate slide events and estimated volumes involved

The new high-resolution airgun data have revealed the distribution of the slide deposits (facies 4) and the facies between them that allows the identification of at least three episodes of slope instability. The geometry of each of the individual failure deposits is very likely lobate in shape with a NW-SE axis, similar to the lobes evident on the seafloor surface, and this is the shape we consider for the deeper slide deposits in order to estimate their volume and areal extent in the absence of a denser network of seismic lines.

On the basis of the seismic profiles, three distinct slide deposits can be identified (slides A, B and C) (Fig. 4).

Slide A is found in the deepest section (between reflectors R2 and R3), separated vertically by about 10 ms thick hemipelagic sediments (facies 1 and/or 5) from slide deposits B1, B2, and C (Fig. 4). The slide deposits vary in thickness from 70 ms down to below the limit of resolution (10 ms) and have an average thickness of 30 ms. Using an acoustic velocity of 1700 m s^{-1} for

moderately consolidated sediments this corresponds to slightly less than 30 m. The area the Slide A deposits occupy is estimated at about 7,500 km^2 (Fig. 9) indicating an approximate volume of ca 200 km^3.

Slide B comprises two parts (B1 and B2) that are highly erosive and are separated laterally by a segment of undisturbed seafloor sediments (Fig. 4b). While they may indicate two separate slide events, they are found at generally the same stratigraphic level. This favours an interpretation where B1 and B2 are part of the same event that bifurcates around a remnant seafloor block or rafted block. Interestingly, a similar pinnacle-like feature is seen on the seafloor vertically above the remnant seafloor block (Fig. 4b). This pinnacle in fact corresponds to an elongate ridge that strikes parallel to the flow direction. It is therefore likely that a similar ridge caused slide B to bifurcate around it. Slide B is 20-60 ms thick, on average 35 ms, which with an acoustic velocity of 1600 m s^{-1} for less consolidated sediments than slide A as this is at shallower stratigraphic level, corresponds to ~30 m. The extent of slide B is more limited than slide A, at 4,500 km^2 and the volume is estimated at ca 125 km^3.

Slide C is characterized by variable internal acoustic character, probably due to different degrees of disintegration and potentially variable lithology (Fig. 4). This deposit is thicker than slide B, at about 120 ms maximum thickness, and not fully cored by the cores (orange line in figs 7 and 8), but has an average thickness of 75 ms, which with the same acoustic velocity as for slide B, yields a thickness of 60 m. Slide C is linked with the lobes that extend on the seafloor downslope of the North Upper Slope scar and the Lower Slope scar (after Georgiopoulou et al. (2013) and has an extent calculated at 6,600 km^2 (Fig. 9). With a volume estimated at ca 400 km^3, slide C is the most voluminous of the three slides.

A fourth event, slide D, is only identifiable in the cores as it is too thin to be resolved by the seismic data (purple line in Figs 7 and 8). It occupies the central downslope area according to its distribution in the cores (Fig 9d). Its deposits suggest that it was a dilute event (further discussion in section 5.1) that generated a turbidity current which flowed ESE and following the seafloor topography was directed southeastward and flowed towards the deepest part of the Rockall Trough (Fig. 9). The average thickness of the event in the study area is 30cm and occupies an area of 4000 km^2 which gives a volume of at least 1.2 km^3 plus the volume of the generated turbidite, which is on average 10cm thick and occupies an area of nearly 5000km^2, i.e. another 0.5 km^3.

The volume of the RBSC was previously calculated by Georgiopoulou et al (2013) based on estimates of the missing sediments from the scars on the Rockall Bank slope. They used two approaches: a “conservative” approach and a more “generous” approach which generated volumes that vary from 265 to 765 km^3 of missing sediments. The present study indicates the total volume of the four slide deposits amounts to ca 725 km^3, which is very close to the “generous” volume of Georgiopoulou et al (2013). This also suggests that the “generous” approach, where a mounded contouritic morphology on the Rockall Bank slope was considered prior to slope collapse, is more realistic than the “conservative” approach in estimating the missing volumes from the scars. However, it should be noted that one of the slides, Slide B, was highly erosive (as discussed above) and therefore the volume of the deposits should exceed the volume of the evacuated sediments, but it is difficult to estimate by how much.

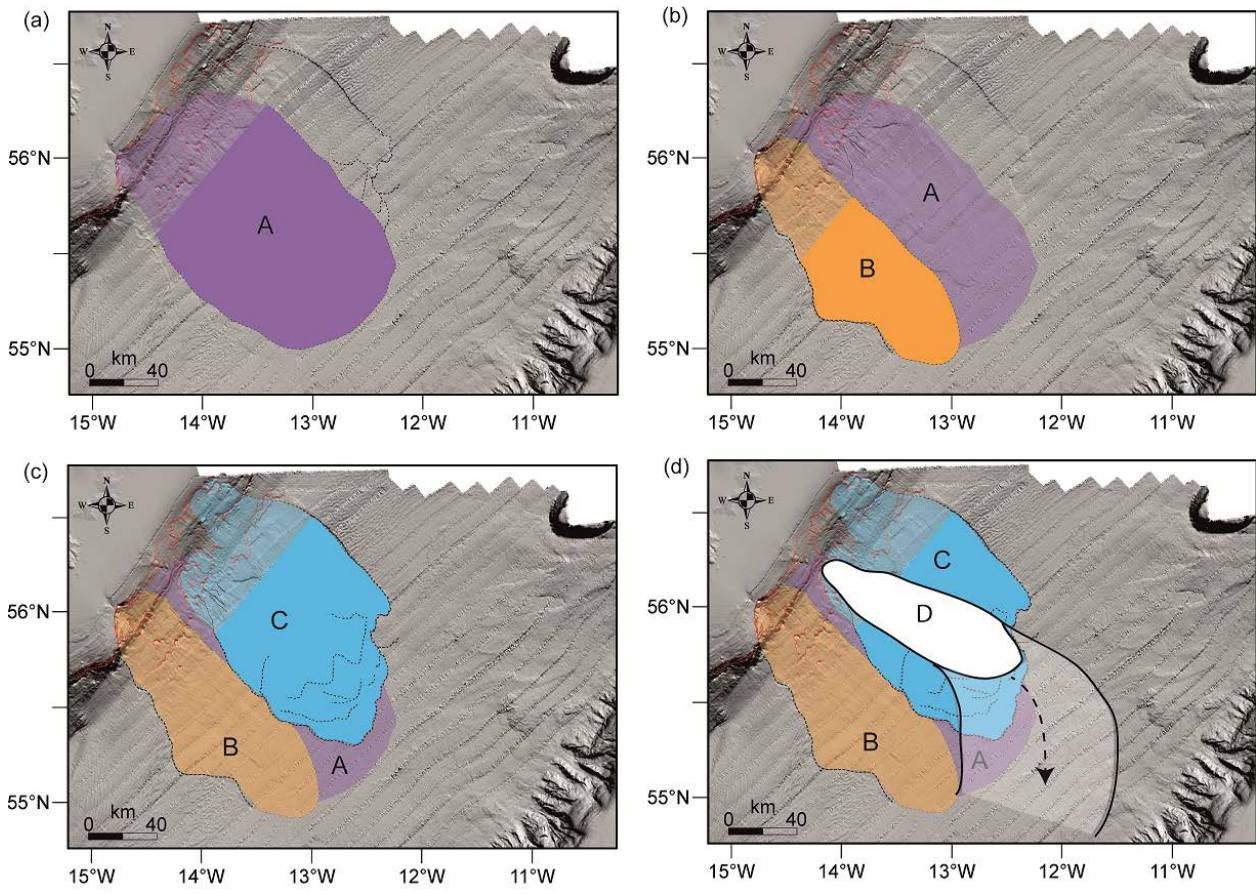

Figure 9. Inferred distribution of slides A, B, C and D based on the seismic and core data as well as the seafloor lobes as expressed on the bathymetry, in the order they took place. The lighter shaded area is the interpreted evacuation area, whereas the darker shaded area is the interpreted depositional area (for each panel the entire area of the earlier slides is lightly shaded).

4.6 Emplacement age of RBSC events

We have calculated a sedimentation rate of about 12 cm ka^{-1} for the last 20 ka for the Rockall Bank slope, and about 2.5 cm ka^{-1} for the deeper Rockall Trough, away from the influence of bottom currents. In order to estimate the ages of the older events we have extrapolated the Rockall Bank sedimentation rate back, assuming constant sedimentation rates, recognizing the uncertainties and potential errors in this approach.

The southernmost deposit, Slide B, is buried under ca 24 m of sediments, which with the above sedimentation rate for the Rockall Bank slope (12 cm ka^{-1}), yields an estimated age of 200 ka. Slide C appears to have deposited at approximately the same stratigraphic level as Slide B, on top of Horizon R2 and adjacent to Slide B (Fig. 4b), probably due to the seafloor topography that Slide B created and then Slide C was routed through it. However, Slide C appears on seismic profiles to be either exposed at the seafloor or if there is a drape on it, it is thinner than the vertical seismic resolution (ca 8 m). By using this thickness we can estimate that slide C is younger than approximately 70 ka. A sub-bottom profile shown in Georgiopoulou et al (2013) (their figure 5) shows recent slide deposits inside the Upper North Slide scar, upslope of Slide C. This would indicate that either Slide C is actually significantly younger than 70 ka or that there has been another, very recent slope collapse in the same area that is not resolved on the seismic data. Indeed, even high-resolution pinger data with 1m vertical resolution do not show slope collapses in the area younger than slide C (Sacchetti et al., (2012b); see their figure 5). However, our core data clearly demonstrate that there has been a more recent failure, slide D, that is deposited only about 0.5 m above slide C and therefore could not be resolved even by the pinger high-resolution data (Figs 7a and 8). The only way to distinguish and establish the distribution of slides C and D is based on the presence (or absence) of the youngest event in the cores.

Core CE11_02 suggests there has been an event, at 20850 cal BP (which is the age of the sample taken 35 cm above the top of the debrite, 17940 cal BP, plus 2910 years that it would take to deposit the 35 cm at 12 cm ka^{-1} sedimentation rate). This event is not found in CE11_01 that was collected from the undisturbed seafloor adjacent to the slide side scarp to the north. It is found in CE11_06 where it has a very similar age of 21750 cal BP. The sandy turbidite that caps the debrite in CE11_06 is also found in CE11_05 although the age in core CE11_05 suggests that this layer of sand is older (28540 cal BP) which would make them uncorrelated. However, this sample was taken from a part of the core that appears to be heavily bioturbated (Fig. 7a) which could have mixed in older material. We suggest that this is the same sandy layer based on its stratigraphic position downcore and the physical properties (Fig. 7a). We considered whether the sandy layer in CE11_04, between sections 1 and 2, also correlated with the sandy layer in CE11_05 and _06, but the physical properties and mineralogy differ (Fig. 7a); in CE11_05 and _06 the sand is foraminifera-dominated and contains rounded and angular lithic grains, whereas in CE11_04 there are very few foraminifera relative to the clastic material which is dominated by glassy angular quartz and dark green lithic fragments. There are also significant differences in the physical properties; crucially the magnetic susceptibility that is a reflection of mineralogy, is higher in CE11_05 and _06, whereas the p-wave velocity and gamma-ray density are higher in CE11_04. Therefore we do not believe the sandy layer correlates across into CE11_04. Core CE14_12 contains a debrite capped by a very thin sand layer dated at 22 ka which correlates well with the other cores. The same event appears in core 09/07_sc1, dated at 21.7 ka (Ovrebo et al., 2005) which is also in very close agreement with the other ages. Cores CE11_03 and CE11_04 contain no debrites but the sedimentary sequence from about 1 m downcore appears disturbed in CE11_03. This could have resulted from slide material buttressing against and ploughing

through the seafloor further upslope and causing in situ deformation of the seafloor. Alternatively, it could be due to the coring procedure. However, there were no problems with the retrieval of CE11_03 and, additionally, if the coring procedure had been responsible then the disturbance should be present along the entire length of the core. As seen on the bathymetric data, cores CE11_03 and CE11_04 were taken from the edges of depositional lobes, i.e. very close to causes of seafloor disturbance. Based on the correlation of the sandy turbidite layer across CE11_05 and _06, it appears that the 22 ka event that generated the debrite/turbidite seen in CE11_05 and _06, may have been responsible for the deformation seen in CE11_03. A similar character is observed at a similar stratigraphic position in core CE14_14 that was taken from the edge of the lobe on the southern side of the complex (Fig. 7a). 08/02_sc1 does not have a deposit that correlates with this event. Nevertheless there is a very sharp contact between contrastingly different hemipelagic sediments (on the basis of colour and lithology) (Fig. 7a). This surface could only have been created by an erosional event and given its stratigraphic position we assign it to the 22 ka event. Given the coincidence of the distribution of the debrite/turbidite in the cores and the distribution of Slide C on the seismic, we believe that slide C is the 22 ka event.

Across the cores from the Lower slope region and in the middle of the slide complex we found a younger debrite-turbidite pair higher in the stratigraphy (Slide D). This event is encountered in cores CE14_13A and CE14_07A, in 08/09_sc1 from Ovrebo et al (2005) and possibly in CE11_03 as a thin turbidite, without a debrite. The age of this event has been determined to be around 10 ka. Absence of this deposit from CE11_05, CE11_06, 08/01_sc1 and 08/02_sc1 (Fig. 8) suggests that this flow followed a narrow ESE trajectory. This event coincides stratigraphically with the T2 turbidite described by Georgiopoulou et al. (2012) in the deeper Rockall Trough.

There appears to be a recent debrite near the top of CE14_07A as well as the top of 78/30_sc1 and a turbidite at the top of CE14_06A, while the entire CE14_08B consists of a debrite deposit capped by a turbidite that is at the top of the core. It is hard to determine whether the deposits in CE14_08B and 78/30_sc1 correlate with the 10 ka event or the even more recent event (Slide E). This latest event does not have a large extent and is not identified in cores further away from the scarps, so it is likely that it is the result of small scarp adjustments.

Slide A is the oldest event. It is difficult to estimate its age with any confidence as there is no way of knowing how much sediment has been removed through erosion by Slides B and C that overlie it. All we can say confidently about Slide A is that it is older than horizon R3 which is probably a few Ma old given the thickness of acoustic facies 5 and the sedimentation rate we have calculated and employed. However, it would be unreasonable to use the same sedimentation rate for the length of period it would have taken to deposit this amount of sediment.

5 Discussion

5.1 Styles of mass transport

Several different types of deposits have been identified in the RBSC, pointing to a wide range of flows in the spectrum of sedimentary flow processes, from dilute to cohesive flows. Core data allow us to assess and compare the flow processes in the last two phases of slope instability in the RBSC.

Slides A and B, being buried deep below the seafloor, and in the absence of their sedimentary record in the cores, cannot be assessed in relation to the flow type save for their acoustic record. The top of Slide A appears blocky. However, the large runout and then thinness of the deposit

suggest that it must have transformed downslope to a more fluid flow that allowed it to spread laterally.

Similarly slide B appears to have been blocky, but less widespread and thicker with pronounced and steep lateral margins. From these characteristics we infer that slide B was probably more concentrated and perhaps flowed more plastically like a debris flow that halted its movement *en masse*, freezing in place. A dilute component that would have deposited a turbidite further downslope cannot be dismissed but there is no evidence for it with the available data.

Slide C appears to have been a bimodal flow, comprised mostly of a cohesive clast-rich debris flow and an accompanying dilute cloud or tail that deposited a thin turbidite as the flow was waning. The turbidity current could have been either high-density or low-density as both can deposit laminated sands (Sumner et al., 2012), which is what has been retrieved in the cores. The runout of the turbidite was not significant though, as we do not encounter it in cores beyond the limits of the slide (Georgiopoulou et al., 2012). The top of this slide appears more smooth relative to slides A and B and we interpret this to mean that the character of this flow was less blocky and maybe more plastic. Similar to slide B, the toe of slide C appears thick, thicker than the body of the slide (Fig. 6), and set within stratified pre-existing sediments as if it buried and confined itself, ploughing through the seafloor. Small-scale thrusts are likely present at the toe (Fig. 6) lending further evidence towards a self-confining type of flow, but not at the extent previously reported for self-confining submarine landslides (Frey Martinez et al., 2005). Further corroborating evidence comes in the form of the sheared section in core CE11_03 that appears as though in situ layers have been locally deformed, possibly due to the lateral pressures emanating from the toe of the slide ploughing through the adjacent seafloor. Different scenarios for modelling of slide C to match the deposits as seen on the bathymetric data reveal that the best fit

resulted when a Bigham rheology was adopted with either a velocity-dependent term or with basal frictional properties (Salmanidou et al., 2018).

Slide D on the other hand appears to have been more dilute, perhaps fully transformed into a turbidity current as indicated by the deposit found in the cores. However, in spite of its dilute nature, this flow did not spread laterally much but did have a long runout and extended mostly downslope as it can be found in a deeper part of the basin (Georgiopoulou et al., 2012). These characteristics suggest that this flow was more rapid and more focused than the previous episodes as it is found along a relatively narrow, elongate axis (Fig. 9d).

Finally, slide E was probably generated by minor secondary scarp spalling that did not produce a large event and the deposits have not gone far from the scarp source. The timing of this event is estimated to be some time in the last millennium as there does not seem to be any substantial drape covering it.

The sequence of events described here based on the depositional data is in general agreement with the sequence of events proposed by Georgiopoulou et al. (2013). However, the present study reveals that these events took place over a considerable period of time. This has also demonstrated the predisposition of the slope for ongoing slope instability and repetitive failure. For example, Slides A and B appear to originate from the same source, perhaps even the same scar, even though Slide B was almost half the size of A.

Attempts to model the flow behaviour of slides A and B, using the same approach as for slide C, demonstrated that this was not possible and the modelled deposits mapped beyond the actual ones (Salmanidou et al., 2018). This was attributed to potentially different rheological properties (Salamanidou et al., 2018). Therefore, the assumption that slide events that occur in the same area and as a result should have the same lithological characteristics, and by extension

393 rheological characteristics, is wrong, at least for this case study, as demonstrated by Salmanidou
394 et al. (2018) and by the different deposits we find in the cores in this study.
395 We also observe that slide events become more frequent in more recent geological time. This
396 does not necessarily reflect an increased rate of slope failure but is more likely a reflection of the
397 increased resolution closer to the seafloor. This could indicate that the thick deposits identified in
398 the deeply buried slides may comprise the composite products of a number of smaller stacked
399 events rather than the result of single large events.
400

401 5.2 Wider implications
402 Early work suggested that the RBSC probably occurred as a single event (Faugères et al., 1981;
403 Flood et al., 1979). Georgiopoulou et al. (2013) examined the scarp morphology at the headwall
404 of the complex and suggested that there may have been several episodes given that the
405 “freshness” or angularity of the scarps varies across the slope, but they were unable to draw any
406 conclusions regarding the timing of events, other than that there were likely to have been
407 significant hiatuses between events as seafloor modifications and healing appeared to have taken
408 place over the older events.
409 In this study, with access to new high resolution seismic and a large number of new cores from
410 the depositional area, we are able to confirm the multi-stage nature of RBSC and cast new light
411 on the emplacement ages and timing between separate events. We have thus demonstrated the
412 long history of instability of the Rockall Bank eastern slope. The youngest slide event took place
413 within the last1000 years but it appears it was very small and did not affect a significant area.
414 The 10ka event (Slide D) was a relatively small event in terms of volume (<2 km^3) but had a
415 very long runout. Slide D was nowhere near as voluminous as the other three but it is significant

nonetheless and demonstrates that more events of these dimensions may be “hidden” in the resolution of the seismic data which has implications for risk assessment studies that consider the repeat interval of submarine slope failures.

The youngest of the large events (Slide C) appears to coincide with the Last Glacial Maximum (LGM), the height of the last glaciation (Clark et al., 2012). Continental margins during glacial periods, when the sea level fell, experienced increased terrigenous input as much of the shelf is exposed and became a sediment source (Johannessen and Steel, 2005). This process cannot have taken place on Rockall Bank as it was not connected to a land mass. A lower sea level may have exposed part of the Rockall Plateau but it could not have been large enough to generate the required large amounts of sediment input. Additionally, the predominant sediment supply for Rockall Bank, as evidenced by seismic profiles and cores, came through bottom currents running parallel to the slope (Georgiopoulou et al., 2013; O'Reilly et al., 2005; Øvrebø et al., 2005; Stoker et al., 2005). However, bottom currents in Rockall Trough are considered to have been slow during glacial times, with seafloor sediment waves barely affected and with minimum winnowing power (Howe, 1996). Previous studies have suggested a combination of rapid sediment accumulation from bottom currents on top of steep basement scarps and slope undercutting by the bottom currents as instability triggering mechanism for this slope (Elliott et al., 2010; Georgiopoulou et al., 2013;Faugères et al. 1981). However, given the timing of the event, could this mechanism have been a primary trigger? It is likely that the slope reacted with some lag time and currents had already destabilized it prior to their weakening and a ground vibration acted as the final trigger.

At 22 ka the British Irish Ice Sheet was starting to decline (Clark et al., 2012). Models predict that isostatic unloading readjustment is experienced in an extensive area beyond the centre of the

ice load, which is about 10° of longitude for the BIIS-sized ice load (Lambeck, 1996). The affected area on Rockall Bank lies a few kilometres inboard of this radius (Fig. 10). During that time (22 ka), the ice sheet was still very close to its maximum extent, still occupying the Irish Shelf (Peters et al., 2016), i.e. most of the ice load was still in place. Models based on relative sea-level data from around Ireland and Scotland show that deglaciation was very rapid *after* 21 ka, and suggestions that it started prior to 21 ka are incompatible with observations (Brooks et al., 2008). If isostatic rebound seismicity was the cause of the 22 ka Rockall Bank slope failure, then this would mean that isostatic rebound response to the BIIS decline was instantaneous, which is unlikely. Therefore we conclude that the generation of the 22 ka slope failure event (slide C) was most probably unrelated to the climatic conditions. However, seismicity, unrelated to isostatic rebound, may have well been responsible for the destabilisation of the 400 km^3 on the Rockall Bank slope.

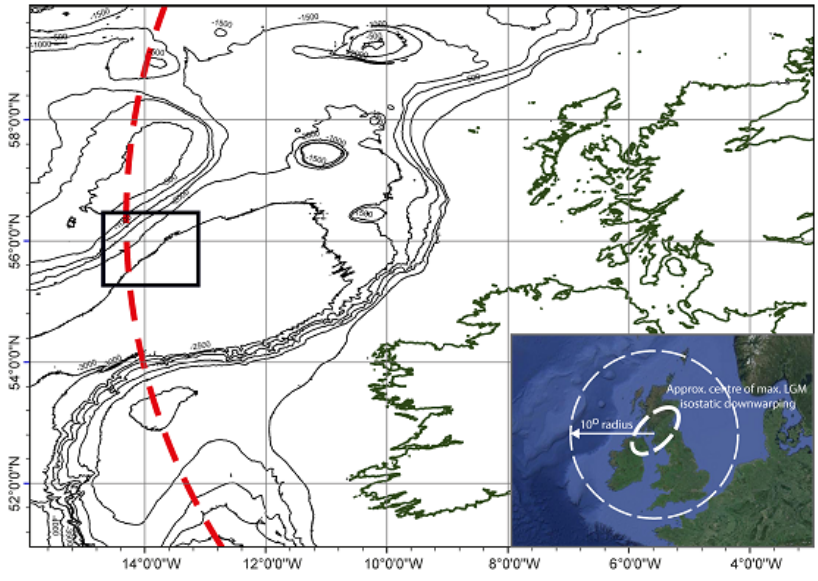

Figure 10. Location of study area (black box) relative to the extent of the area affected by isostatic downwarping (red dashed line) according to Lambeck (1996).

Seismicity due to isostatic rebound may have been responsible for the more recent event. The initiation area for this event is also within the area of influence of the main sweeping bottom current in the area that is strong enough to incise a moat at the base of slope of Rockall Bank. Whether or not slides C or D could have generated tsunamis is beyond the scope of the present project. Slide C was modelled by Salmanidou et al. (2017) and it was shown to have generated a 5-10m high tsunami that traversed Rockall Trough and impacted on the Co. Mayo coast, NW Ireland. However, given the timing, it is unlikely it reached the coast, having encountered the BIIS first, which at 22 ka was still occupying the Irish shelf (Clark et al., 2012; Peters et al., 2016; Sacchetti et al., 2012b). The ice shelf would likely have dampened the effect of the tsunami wave. However, considering that the triggering mechanism is probably unrelated to the climate (beginning of deglaciation), analysis of likely future risk from the repetition of such an event, especially when the affected slope has not been fully evacuated and potential incipient scarps can be seen on the seafloor (Georgiopoulou et al., 2013 and their figure 6), and at least one, albeit much smaller event has taken place since, it is worthy of further study.

For tsunami risk assessments it is imperative that studies like the current one are undertaken prior to modelling, in order to separate and distinguish the different events that constitute a slide complex, otherwise the risk may be overestimated or even underestimated. Very large events (several 100s of km^3) that would generate more destructive tsunamis tend to have large recurrence intervals and therefore, while the hazard exists, the risk may be considered small. However, smaller- and medium-scale landslides (10s to a few 100s of km^3) will have shorter recurrence intervals and therefore the risk increases. Of course there are other factors that need to be considered, such as sedimentation rates and replenishment of the slope with enough sediment before another slide might take place.

This study has demonstrated that (a) it is more likely that large buried slide events comprise multiple smaller stacked events, and (b) slide events originating on the same slope, with the same sediment source may have very different flow behaviour probably because each slide creates new conditions for the slope and the seafloor that gets traversed by the following slide. Perhaps the later slides tap into different lithologies or even remobilize earlier slide deposits, which, in combination with the changed topography and the increased bed roughness, may have significant effects in determining the flow behaviour, allowing younger slides to disaggregate more, complicating further forecasting future slide behaviours and tsunami modelling.

6 Conclusions

Using a set of newly-acquired high-resolution seismic profiles and gravity cores from the depositional area of the Rockall Bank Slide Complex we have been able to demonstrate that:

- The complex comprises at least three large-scale slides of 200, 125 and 400 km^3 each, slides A, B and C in order of occurrence from oldest to youngest.
- Slides A and B occupy the southernmost part of the complex, while Slide C extends across the middle and northernmost parts. This suggests that different parts of the slope were unstable, although the southern scarp appears to have been unstable on at least two occasions.
- The most recent events, Slides C, D and E are dated at 22 ka, 10 ka and within the last 1000 years respectively.
- Based on the three most recent events, the recurrence period for slope instability in Rockall Bank is about 10 ka, which might suggest that currently the slope is unstable.
- The concurrence of slide C with the beginning of deglaciation of the BIIS appears to be coincidental.

- Multiple events from the same source area can and do generate events with different flow behaviours.

7 Acknowledgments

Bathymetric data used in this paper can be found on www.infomar.ie. New core raw data (core descriptions and MSCL measurements) and all CE11011 seismic profiles are provided as supplemental material. Other cores used are published in literature. This study has been supported by the Irish National Development Plan Marine Research Sub-Programme. We wish to express our gratitude to the Officers, Scientists and Crew of Celtic Explorer expeditions CE11011 and CE14011 for all the help and good times. AG would like to acknowledge the Griffith Geoscience Awards and the Geological Survey Ireland Short Call awards (Grant 2015-sc-036). Seismic data collection was supported by the Deutsche Forschungsgemeinschaft (Grant KR2222/14-1).

References

Brooks, A.J., Bradley, S.L., Edwards, R.L., Milne, G.A., Horton, B., and Shennan, I. (2008). Postglacial relative sea-level observations from Ireland and their role in glacial rebound modelling. *Journal of Quaternary Science*, 23, 175-192, https://doi.org/10.1002/jqs.1119

Bull, S., Cartwright, J., and Huuse, M. (2009). A review of kinematic indicators from mass-transport complexes using 3D seismic data. *Marine and Petroleum Geology*, 26, 1132-1151, https://doi.org/10.1016/j.marpetgeo.2008.09.011

Clark, C.D., Hughes, A.L.C., Greenwood, S.L., Jordan, C., and Sejrup, H.P. (2012). Pattern and timing of retreat of the last British-Irish Ice Sheet. *Quaternary Science Reviews*, 44, 112-146, https://doi.org/10.1016/j.quascirev.2010.07.019

Elliott, G.M., Shannon, P.M., Haughton, P.D.W., and Øvrebø, L.K. (2010). The Rockall Bank Mass Flow: Collapse of a moated contourite drift onlapping the eastern flank of Rockall Bank, west of Ireland. *Marine and Petroleum Geology*, 27, 92-107, https://doi.org/10.1016/j.marpetgeo.2009.07.006

Faugères, J.C., Gonthier, E., Grousset, F., and Poutiers, J. (1981). The Feni Drift: The importance and meaning of slump deposits on the Eastern slope of the Rockall Bank. *Marine Geology*, 40, M49-M57, https://doi.org/10.1016/0025-3227(81)90138-9

Faugères, J.C., Stow, D.A.V., Imbert, P., and Viana, A. (1999). Seismic features diagnostic of contourite drifts. *Marine Geology*, 162, 1-38, https://doi.org/10.1016/S0025-3227(99)00068-7

Flood, R.D., Hollister, C.D., and Lonsdale, P. (1979). Disruption of the Feni sediment drift by debris flows from Rockall Bank. *Marine Geology*, 32, 311-334, https://doi.org/10.1016/0025-3227(79)90070-7

Frey Martinez, J., Cartwright, J.A., and Hall, B. (2005). 3D seismic interpretation of slump complexes: examples from the continental margin of Israel. *Basin Research*, 17, 83-108, https://doi.org/10.1111/j.1365-2117.2005.00255.x

Georgiopoulou, A., Benetti, S., Jones, S.M., and Wall, D. (2010). RV Celtic Explorer CE10008 cruise report, 3rd - 17th June, 2010 (Galway-Galway): Glacial and non-glacial sediment transport and seismic oceanography in the Rockall Trough, NE Atlantic, *Cruise Reports*. Marine Institute, Galway, p. 24.

Georgiopoulou, A., Benetti, S., Shannon, P.M., Haughton, P.D.W., and McCarron, S. (2012). Gravity flow deposits in the deep Rockall Trough, Northeast Atlantic, in: Yamada, Y., Kawamura, K., Ikehara, K., Ogawa, Y., Urgeles, R., Mosher, D.C., Chaytor, J.D., Strasser, M. (Eds.), Submarine mass movements and their consequences, Advances in Natural and Technological Hazards Research. Springer, Dordrecht Heidelberg London New York, pp. 695-707.

Georgiopoulou, A., Shannon, P.M., Sacchetti, F., Haughton, P.D.W., and Benetti, S. (2013). Basement-controlled multiple slope collapses, Rockall Bank Slide Complex, NE Atlantic. *Marine Geology*, 336, 198-214, https://doi.org/10.1016/j.margeo.2012.12.003.

Harkness, D. (1983). The extent of the natural 14C deficiency in the coastal environment of the United Kingdom. Proceedings of the First International Symposium 14C and Archaeology PACT 8, 351-364.

Holmes, R., Long, D., and Dodd, L.R. (1998). Large-scale debrites and submarine landslides on the Barra Fan, west of Britain. Geological Society, London, *Special Publications*, 129, 67-79.

Howe, J.A. (1996). Turbidite and contourite sediment waves in the northern Rockall trough, north Atlantic Ocean. *Sedimentology*, 43, 219-234, https://doi.org/10.1046/j.1365-3091.1996.d01-1.x

Hunt, J.E., Wynn, R.B., Masson, D.G., Talling, P.J., and Teagle, D.A.H. (2011). Sedimentological and geochemical evidence for multistage failure of volcanic island landslides: A case study from Icod landslide on north Tenerife, Canary Islands. *Geochemistry, Geophysics, Geosystems*, 12, Q12007, https://doi.org/10.1029/2011GC003740

Johannessen, E.P., & Steel, R.J. (2005). Shelf-margin clinoforms and prediction of deepwater sands. *Basin Research*, 17, 521-550, https://doi.org/10.1111/j.1365-2117.2005.00278.x

Lambeck, K. (1996). Glaciation and sea-level change for Ireland and the Irish Sea since Late Devensian/Midlandian time. *Journal of the Geological Society, London*, 153, 853-872, https://doi.org/ 10.1144/gsjgs.153.6.0853

O'Reilly, B.M., Readman, P.W., and Shannon, P.M. (2005). Slope failure, mass flow and bottom current processes in the Rockall Trough, offshore Ireland, revealed by deep-tow sidescan sonar. *First Break*, 23, 45-50.

590 O'Reilly, B.M., Shannon, P.M., and Readman, P.W. (2007). Shelf to slope sedimentation
591 processes and the impact of Plio-Pleistocene glaciations in the northeast Atlantic, west of
592 Ireland. *Marine Geology*, 238, 21-44, https://doi.org/10.1016/j.margeo.2006.12.008
593
594 Øvrebø, L.K., Haughton, P.D.W., and Shannon, P.M., (2005). Temporal and spatial variations in
595 late Quaternary slope sedimentation along the undersupplied margins of the Rockall Trough,
596 offshore west Ireland. *Norwegian Journal of Geology*, 85, 279-294.
597
598 Peters, J.L., Benetti, S., Dunlop, P., Ó Cofaigh, C., Moreton, S.G., Wheeler, A.J., and Clark,
599 C.D. (2016). Sedimentology and chronology of the advance and retreat of the last British-Irish
600 Ice Sheet on the continental shelf west of Ireland. *Quaternary Science Reviews*, 140, 101-124,
601 https://doi.org/10.1016/j.quascirev.2016.03.012.
602
603 Reimer, P.J., Bard, E., Bayliss, A., Beck, J.W., Blackwell, P.G., Ramsey, C.B., et al. (2013).
604 IntCal13 and Marine13 Radiocarbon Age Calibration Curves 0–50,000 Years cal BP.
605 *Radiocarbon*, 55, 1869-1887, https://doi.org/10.2458/azu_js_rc.55.16947
606
607 Sacchetti, F., Benetti, S., Georgiopoulou, A., Dunlop, P., and Quinn, R. (2011). Geomorphology
608 of the Irish Rockall Trough, North Atlantic Ocean, mapped from multibeam bathymetric and
609 backscatter data. *Journal of Maps*, 2011, 60-81, https://doi.org/10.4113/jom.2011.1157
610
611 Sacchetti, F., Benetti, S., Georgiopoulou, A., Shannon, P.M., O'Reilly, B.M., Dunlop, P., et al.
612 (2012a). Deep-water geomorphology of the glaciated Irish margin from high-resolution marine

geophysical data. *Marine Geology*, 291-294, 113-131, https://doi.org/10.1016/j.margeo.2011.11.011

Sacchetti, F., Benetti, S., Quinn, R., and Ó Cofaigh, C. (2012b). Glacial and post-glacial sedimentary processes in the Irish Rockall Trough from an integrated acoustic analysis of near-seabed sediments. *Geo-Marine Letters*, 33, 49-66, https://doi.org/10.1007/s00367-012-0310-2

Salmanidou, D.M., Georgiopoulou, A., Guillas S., and Dias, F. (2018). Rheological considerations for the modelling of submarine sliding at Rockall Bank, NE Atlantic. *Physics of fluids*, 30, 030705 https://doi.org/10.1063/1.5009552

Salmanidou, D.M., Guillas, S., Georgiopoulou, A., and Dias, F. (2017). Statistical emulation of landslide-induced tsunamis at the Rockall Bank, NE Atlantic. *Proceedings of the Royal Society A-Mathematical Physical and Engineering Sciences*, 473(2200), 20170026, https://doi.org/10.1098/rspa.2017.0026

Stoker, M.S. (1998). Sediment-drift development on the continental margin off NW Britain, in: Stoker, M.S., Evans, D., Cramp, A. (Eds.), Geological processes on continental margins: sedimentation, mass-wasting and stability. *Geological Society Special Publication*, 129, London, pp. 229-254.

Stoker, M.S., Akhurst, M.C., Howe, J.A., and Stow, D.A.V. (1998). Sediment drifts and contourites on the continental margin off northwest Britain. *Sedimentary Geology*, 115, 33-51, https://doi.org/10.1016/S0037-0738(97)00086-9

Stoker, M.S., Praeg, D., Hjelstuen, B.O., Laberg, J.S., Nielsen, T., and Shannon, P.M. (2005). Neogene stratigraphy and the sedimentary and oceanographic development of the NW European Atlantic margin. *Marine and Petroleum Geology*, 22, 977-1005, https://doi.org/10.1016/j.marpetgeo.2004.11.007

Stoker, M.S., van Weering, T.C.E., and Svaerdborg, T. (2001). A Mid- to Late Cenozoic tectonostratigraphic framework for the Rockall Trough, in: Shannon, P.M., Haughton, P.D.W., Corcoran, D.V. (Eds.), The petroleum exploration of Ireland's offshore basins. *Geological Society Special Publication*, 188, London, pp. 411-438.

Stuiver, M., & Reimer, P.J. (1986). A computer program for radiocarbon age calibration. *Radiocarbon*, 28, 1022-1030.

Unnithan, V., Shannon, P.M., McGrane, K., Readman, P.W., Jacob, A.W.B., Keary, and R., Kenyon, N.H. (2001). Slope instability and sediment redistribution in the Rockall Trough: constraints from GLORIA, in: Shannon, P.M., Haughton, P.D.W., Corcoran, D.V. (Eds.), The petroleum exploration of Ireland's offshore basins. *Geological Society Special Publication*, 188, London, pp.439-454.

van Weering, T.C.E., & de Rijk, S. (1991). Sedimentation and climate-induced sediments on Feni Ridge, Northeast Atlantic Ocean. *Marine Geology*, 101, 49-69, https://doi.org/10.1016/0025-3227(91)90062-9

Ward, S.N., & Day, S. (2001). Cumbre Vieja Volcano-Potential Collapse and tsunami at La Palma, Canary Islands. *Geophysical Research Letters*, 28, 3397-3400, https://doi.org/10.1029/2001GL013110

Wynn, R.B., & Stow, D.A.V. (2002). Classification and characterisation of deep-water sediment waves. *Marine Geology*, 192, 7-22, https://doi.org/10.1016/S0025-3227(02)00547-9.